Higher-Order Modal Dispersion in Graded-Index Multimode Fiber

Mahdieh B. Shemirani and Joseph M. Kahn, *Fellow, IEEE*

Abstract—Previously, we proposed a field-coupling model for propagation in graded-index multimode fiber (MMF), analogous to the principal states model for polarization-mode dispersion (PMD) in single-mode fiber. That model was based on the concept of first-order principal modes, which have well-defined group delays that depend on the strength of the mode coupling. That first-order model predicts a linear relationship between the intensity waveforms at the MMF input and output. Here, we extend that model to account for higher order modal dispersion. The higher-order model predicts several effects analogous to higher-order PMD: pulse broadening, filling-in between peaks of the pulse response, depolarization and pattern blurring at the MMF output, and a nonlinear relationship between input and output intensity waveforms.

Index Terms—Depolarization, field-coupling model, higher-order modal dispersion, higher-order principal modes (PMs), impulse response, multimode fiber (MMF), polarization-mode dispersion (PMD), power nonlinearity, principal state of polarization (PSP), pulse broadening.

I. INTRODUCTION

IN a multimode fiber (MMF), different modes generally propagate with different group delays (GDs), an effect known as modal dispersion. Fiber imperfections, such as index inhomogeneity, core ellipticity and eccentricity, and bends, introduce coupling between modes, an effect known as mode coupling. Because of mode coupling, even if a light pulse is launched into a single mode, it tends to couple to other modes, leading to a superposition of several pulses at the MMF output. This causes intersymbol interference and a reduction of fiber bandwidth.

Traditionally, modal dispersion and coupling in MMF have been described using power-coupling models [1]–[6]. These models assume that mode coupling causes packets of energy to hop from one ideal mode to another, while these modes and their GDs remain unperturbed by the coupling. Power-coupling models have been used to explain the power distribution among different modes [1] and its dependence on fiber length [2], [3], dependence of fiber bandwidth on fiber length [1], narrowing of delay spread in plastic fibers [4], pulse broadening [4], [5], and an observed filling-in between peaks of the pulse response [6]. However, power-coupling models fail to explain certain effects, such as polarization dependence of the pulse response [7].

By contrast, field-coupling models have been used extensively to study polarization-mode dispersion (PMD) in single-mode fiber (SMF) [8]–[11]. A well-known method to model (or to physically emulate) PMD is to concatenate an alternating sequence of random birefringent elements and random polarization rotators [12], [13]. Such a model can yield Jones matrices with the complex frequency dependence characteristic of PMD. For many purposes, it is useful to classify PMD in terms of its order. In first-order PMD, the phase of the Jones matrix is assumed to vary linearly with frequency. Eigenvector expansion yields two principal states of polarization (PSPs), which are mutually orthogonal and correspond to states of polarization and GDs that are independent of frequency [9]. In higher-order PMD, the Jones matrix and the PSPs exhibit more complicated frequency dependence. At least four different approaches have been used to study higher-order PMD analytically [14]–[17]. They differ in terms of what is assumed to be known about the Jones matrix and in the way the frequency dependence is expanded. Ferreira [18] has compared these various approaches.

A field-coupling model was first applied to MMF in [19], which generalized the model for first-order PMD in SMF [9]. A GD operator was derived in [19] from the propagation operator. The eigenvectors of the GD operator, called principal modes (PMs), were shown to be mutually orthogonal, and to have field patterns and GDs that are independent of frequency to first order. Like the PSPs in SMF, the PM field patterns and GDs are dependent upon mode coupling, in contrast to assumptions of power-coupling models. This field-coupling model was used to study propagation in graded-index MMF in [20]. While in real fibers, spatial- and polarization-mode coupling can arise from many sources, in [20], bends and angular twists were employed to induce these couplings. An MMF was modeled by concatenating numerous short sections, each having random curvature and random angular orientation. Given a random realization of the curvatures and angular orientations, the propagation matrix was computed and used to obtain the first-order PMs and their GDs. The study in [20] explained for the first time the polarization dependence of the pulse response [7] and provided an alternative explanation for the reduced GD spread in highly perturbed fibers [4]. It also confirmed a linear dependence of GD spread on MMF length in the low-coupling regime and a square-root dependence on length in the high-coupling regime.

Recently, the intensity pulse response of silica MMFs was measured with high dynamic range [6]. It was found that most of the energy arrives in the peaks corresponding to GDs of discrete mode groups, but some energy is observed at intermediate GDs, leading to filling-in of the pulse response. These results were explained using a power-coupling model, which shows that the fraction of energy at intermediate GDs increases as the

The authors are with the Department of Electrical Engineering, Stanford University, Stanford, CA 94305-9505 USA (e-mail: mahdieh@stanford.edu; jmk@ee.stanford.edu).

mode coupling strength increases. The results in [6] cannot be explained using the field-coupling model in [20], because in that first-order model, all of the energy must arrive in one of the first-order PMs, which have well-defined GDs.

In this paper, we show that the results in [6] can be explained by extending the field-coupling model of [20] to include higher-order modal dispersion, which is analogous to higher-order PMD in SMF. Using the extended model, we show that to first order in frequency, no filling-in of the pulse response is observed, while higher-order effects cause a filling-in that increases with the strength of mode coupling. We show that to first order, the relationship between the input and output intensity waveforms is linear, while higher-order effects cause this relationship to become nonlinear, as in SMF with chromatic dispersion (CD) or higher-order PMD [17], effects that cause the phase response to depend on ω^2 and higher powers of ω. Similar to higher-order PMD, which causes polarization-dependent CD and depolarization, higher-order modal dispersion causes pulse broadening, depolarization, and field-pattern blurring at the output of an MMF.

The remainder of this paper is organized as follows. In Section II, using an exponential expansion of the propagation operator similar to one used for Jones matrices in SMF [14], we study the properties of first- and second-order modal dispersion. The PMs and their GDs are found up to second order in frequency. We show that second-order modal dispersion causes pulse broadening and a nonlinear relationship between input and output intensity waveforms. In Section III, we present numerical calculations for a silica MMF considering all orders of perturbation. We model the fiber as a concatenation of short sections, each of which is curved and angularly twisted with respect to adjacent sections. We illustrate some of the properties of higher-order modal dispersion, including filling-in of the pulse response, a nonlinear relationship between input and output intensity waveforms, and output depolarization and pattern blurring. We present our conclusions in Section IV.

II. FIRST- AND SECOND-ORDER THEORY

Given a Jones matrix describing PMD in SMF, there are several different methods for finding the higher-order PSPs [14]–[17]. Here, given a propagation operator describing an MMF, we use an approach similar to [14] to find the first- and second-order PMs.

A. Propagation Operator Expansion

In this section, in order to study first- and second-order modal dispersion analytically and gain intuition on its *qualitative* properties, we use an exponential expansion of the propagation operator. This is analogous to the expansion of the Jones matrix used to study second-order PMD in SMF [14]. The exponential expansion is known to have limitations, e.g., by stopping the expansion at second order, the differential GD becomes unbounded at large frequency offsets [16], [18]. Nonetheless, the exponential expansion is useful for two reasons. It is consistent with our previous definition of first-order PMs [19], [20], unlike the Taylor series expansion used in [17].

Also, the high complexity of the propagation matrix in MMF[1] would make it difficult to perform analyses similar to those in [15] and [16]. In Section III, in order to perform *quantitative* study of higher-order modal dispersion, we present numerical computations considering all orders of perturbation.

Using a modified version of the exponential expansion of [14], we can write the frequency-perturbed propagation operator as:

$$U(\omega_0 + \Omega) = U^{(0)} \exp\left(-j\Omega F^{(1)}\right)$$
$$\times \exp\left(\frac{1}{2}\Omega^2 F^{(2)}\right) \exp\left(j\frac{1}{6}\Omega^3 F^{(3)}\right) \cdots \quad (1)$$

Here, $U^{(0)}$ is the zeroth-order propagation operator calculated at ω_0. For a fiber with M modes in two polarizations, $F^{(k)}(k = 1, 2, 3, \ldots)$ are the kth-order $M \times M$ characteristic operators of modal dispersion, which can be found by successively differentiating (1) with respect to Ω and substituting $\Omega = 0$.

The eigenvectors and eigenvalues of $F^{(k)}$ are called the frequency-independent kth-order input PMs $P_i^{(k)}$ and their GDs $\tau_i^{(k)}$. We can write (1) in a more useful form [14] by observing that if A is a nonsingular matrix with eigenvalues $\alpha_k(k = 1, 2, \ldots, M)$, then e^A and A have the same eigenvectors, and the eigenvalues of e^A are e^{α_k}. Hence,

$$U(\omega_0 + \Omega) = U^{(0)} \left|P^{(1)}\right\rangle Q^{(1)}(\Omega)$$
$$\times \left\langle P^{(1)}\right|\left|P^{(2)}\right\rangle Q^{(2)}(\Omega)\left\langle P^{(2)}\right| \cdots \quad (2)$$

where $Q^{(k)}$ is a diagonal matrix with $Q_{ii}^{(k)} = \exp(-(1/k!)(j\Omega)^k \tau_i^{(k)})$ for $i = 1, \ldots, M$.[2]

B. First-Order Modal Dispersion

To first order in Ω, we can write the propagation operator as

$$U^{(1)}(\omega_0 + \Omega) = U^{(0)} e^{-j\Omega F^{(1)}} \quad (3)$$

where the GD operator $F^{(1)}$ is given by

$$F^{(1)} = j\left(U^{(0)}\right)^{-1}\frac{\partial U}{\partial \Omega}\bigg|_{\Omega=0}. \quad (4)$$

We consider an input field with intensity (instantaneous power) waveform $S_{\text{in}}(t)$

$$E_{\text{in}}(t) = \sqrt{S_{\text{in}}(t)}|a\rangle e^{j\omega_0 t} \quad (5)$$

[1]A Jones matrix can be described by only two complex parameters, making it possible to obtain simple closed-form solutions for the state of polarization and elements of Jones matrices [17]. The propagation matrix of an MMF, however, is described by M parameters, where M is the number of modes in two polarizations, making it difficult to obtain closed-form expressions for the modes and for elements of the propagation matrix.

[2]We use Heisenberg notation for the matrix of PMs: $|P^{(k)}\rangle = \left[|P_1^{(k)}\rangle \cdots |P_M^{(k)}\rangle\right]$. We define a "ket-bra" product as: $|P\rangle\langle P| = \sum_i |P_i\rangle\langle P_i|$. We also define a "bra-ket" product of two operators as:

$$\langle P \| P \rangle = \begin{bmatrix} \langle P_1 | P_1 \rangle & \cdots & \langle P_1 \| P_M \rangle \\ \vdots & \ddots & \vdots \\ \langle P_M \| P_1 \rangle & \cdots & \langle P_M | P_M \rangle \end{bmatrix}.$$

where $|a\rangle$ is the launched field pattern in an arbitrary basis (e.g., the basis of ideal modes) and $\langle a \, | \, a \rangle = 1$. We assume that the spatial pattern does not change as we modulate the intensity by $S_{\text{in}}(t)$. The output field of this first-order system can be written as

$$E_{\text{out}}^{(1)}(t) = \text{FT}^{-1} \left\{ U^{(0)} \left| P^{(1)} \right\rangle Q^{(1)}(\Omega) \right.$$
$$\left. \times \left\langle P^{(1)} \right| \text{FT}\{\sqrt{S_{\text{in}}(t)}\} |a\rangle \right\} e^{j\omega_0 t} \quad (6)$$

where $\text{FT}\{\ \}$ denotes the Fourier transform operator.

We can rearrange (6) into a more familiar form knowing that PMs are independent of frequency

$$E_{\text{out}}^{(1)}(t) = U^{(0)} \left| P^{(1)} \right\rangle \text{FT}^{-1}$$
$$\times \left\{ Q^{(1)}(\Omega) \text{FT}\{\sqrt{S_{\text{in}}(t)}\} \right\} \left\langle P^{(1)} \right| |a\rangle e^{j\omega_0 t} \quad (7)$$

where $\langle P^{(1)} \| a \rangle$ is the input-mode pattern projected onto the basis of PMs and $U^{(0)}|P^{(1)}\rangle$ is a matrix of the output PMs, which transforms the output field pattern back to the basis for which $|a\rangle$ is defined. Defining the operator

$$D^{(1)}(t) = \text{FT}^{-1} \left\{ Q^{(1)}(\Omega) \text{FT}\{\sqrt{S_{\text{in}}(t)}\} \right\} e^{j\omega_0 t} \quad (8)$$

the first-order output intensity waveform can be written as

$$S_{\text{out}}^{(1)}(t) = \left| E_{\text{out}}^{(1)}(t) \right|^2$$
$$= \langle a| \left\{ \left| P^{(1)} \right\rangle D^{(1)}(t)^H D^{(1)}(t) \left\langle P^{(1)} \right| \right\} |a\rangle. \quad (9)$$

The superscript H denotes the Hermitian conjugate. We can write the elements of the operator $D^{(1)}(t)$ as

$$d_{ii}^{(1)}(t) = \text{FT}^{-1} \left\{ \text{FT}\{\sqrt{S_{\text{in}}(t)}\} e^{-j\Omega \tau_i^{(1)}} \right\} e^{j\omega_0 t}$$
$$= \sqrt{S_{\text{in}}\left(t - \tau_i^{(1)}\right)} e^{j\omega_0 t}, \qquad \text{for } i = 1, \ldots, M$$

which gives

$$D^{(1)}(t)^H D^{(1)}(t)$$
$$= \begin{bmatrix} S_{\text{in}}\left(t - \tau_1^{(1)}\right) & & 0 \\ & \ddots & \\ 0 & & S_{\text{in}}\left(t - \tau_M^{(1)}\right) \end{bmatrix}. \quad (10)$$

Hence, the output intensity waveform (9) can be written in the form

$$S_{\text{out}}^{(1)}(t) = \left| E_{\text{out}}^{(1)}(t) \right|^2 = \sum_{k=1}^{M} \left| \mu_k^{(1)} \right|^2 S_{\text{in}}\left(t - \tau_k^{(1)}\right) \quad (11)$$

where $\mu^{(1)} = \langle P^{(1)} \, | \, a \rangle$. The output waveform (11) consists of copies of the nonnegative input waveform, delayed by the first-order GDs $\tau_k^{(1)}$, and scaled by nonnegative gains $|\mu_k^{(1)}|^2$, which satisfy $\sum |\mu_k^{(1)}|^2 = 1$. Thus, to first order in frequency, the system described by $U^{(1)}(\omega_0 + \Omega)$ exhibits a linear relationship between input and output intensity waveforms. If we let the input consist of an isolated short pulse, we can interpret (11) as the first-order intensity pulse response of the MMF. This pulse response consists of a set of scaled pulses delayed by discrete GDs. It exhibits no filling-in between these discrete pulses.

C. Second-Order Modal Dispersion

To second order in Ω, the propagation operator U is given by

$$U^{(2)}(\omega_0 + \Omega) = U^{(0)} \exp\left(-j\Omega F^{(1)}\right) \exp\left(\frac{1}{2}\Omega^2 F^{(2)}\right) \quad (12)$$

where the second-order GD operator $F^{(2)}$ can be found as

$$F^{(2)} = j\left(U^{(0)}\right)^{-1} \left. \frac{\partial^2 U}{\partial \Omega^2} \right|_{\Omega=0} + \left(F^{(1)}\right)^2. \quad (13)$$

Up to second order, the output field is found to be

$$E_{\text{out}}^{(2)}(t) = U^{(0)} \left| P^{(1)} \right\rangle \ldots$$
$$\times \text{FT}^{-1} \left\{ Q^{(1)}(\Omega) \left\langle P^{(1)} \right| \left| P^{(2)} \right\rangle \right.$$
$$\times \left. Q^{(2)}(\Omega) \text{FT}\{\sqrt{S_{\text{in}}(t)}\} \right\} e^{j\omega_0 t} \ldots$$
$$\times \left\langle P^{(2)} \right| |a\rangle. \quad (14)$$

Defining the second-order PM propagator, which converts the output to the basis of first-order PMs

$$Z^{(2)}(\Omega) = \left\langle P^{(1)} \right| \left| P^{(2)} \right\rangle Q^{(2)}(\Omega) \text{FT}\{\sqrt{S_{\text{in}}(t)}\} \quad (15)$$

(14) can be written as

$$E_{\text{out}}^{(2)}(t) = U^{(0)} \left| P^{(1)} \right\rangle$$
$$\times \text{FT}^{-1} \left\{ Q^{(1)}(\Omega) Z^{(2)}(\Omega) \right\} e^{j\omega_0 t} \left\langle P^{(2)} \right| |a\rangle. \quad (16)$$

In (16), the input pattern is first projected into the basis of second-order PMs. Then, these PMs are acted on by the operator $Z^{(2)}(\Omega)$, so that each term is scaled by the second-order filter $Q^{(2)}(\Omega)$, and then the filtered second-order PMs are transformed by $\langle P^{(1)} \| P^{(2)} \rangle$ from the basis of second-order PMs to the basis of first-order PMs. As a result of this transformation, $Z^{(2)}(\Omega)$ is not a diagonal matrix, neither in terms of $|P^{(1)}\rangle$, nor in terms of $|P^{(2)}\rangle$, and there is mixing between the different
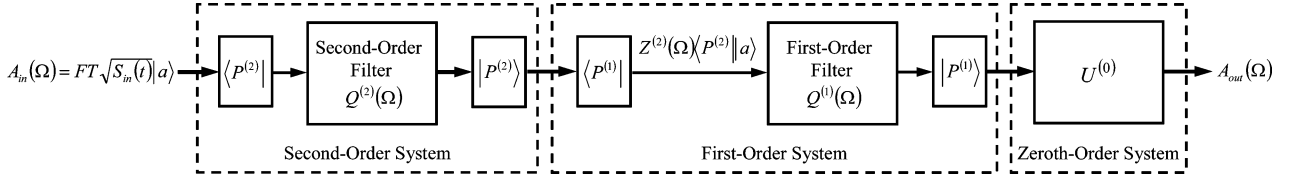
Fig. 1. Representation of MMF in terms of zeroth-, first- and second-order systems.

first-order PMs. Finally, the results are scaled by the first-order filter $Q^{(1)}(\Omega)$. This is illustrated in Fig. 1.[3]

Defining

$$
D^{(2)}(t) = \mathrm{FT}^{-1}\left\{Q^{(1)}(\Omega)Z^{(2)}(\Omega)\right\}e^{j\omega_0 t}
$$

$$
= \begin{bmatrix} Z_{11}^{(2)}\left(t-\tau_1^{(1)}\right) & \cdots & Z_{1M}^{(2)}\left(t-\tau_1^{(1)}\right) \\ \vdots & \ddots & \vdots \\ Z_{M1}^{(2)}\left(t-\tau_M^{(1)}\right) & \cdots & Z_{MM}^{(2)}\left(t-\tau_M^{(1)}\right) \end{bmatrix} e^{j\omega_0 t} \tag{17}
$$

we can write the output intensity waveform up to second order as

$$
\begin{aligned}
S_{\mathrm{out}}^{(2)}(t) &= \left|E_{\mathrm{out}}^{(2)}(t)\right|^2 \\
&= \langle a| \left\{\left|P^{(2)}\right\rangle D^{(2)}(t)^H D^{(2)}(t)\left\langle P^{(2)}\right|\right\}|a\rangle.
\end{aligned} \tag{18}
$$

Theorem 2-1: To second order, the output intensity waveform exhibits pulse broadening.

Proof: Defining the vector of the input projected onto the second-order PMs $\mu^{(2)} = \langle P^{(2)}\|a\rangle$, we find the output of the second-order system projected onto the first-order PMs to be (see Fig. 1)

$$
\begin{aligned}
Z^{(2)}(\Omega)\left\langle P^{(2)}\right||a\rangle &= \left\langle P^{(1)}\right|\left|P^{(2)}\right\rangle \\
&\times \begin{bmatrix} \mathrm{FT}\{\sqrt{S_{\mathrm{in}}(t)}\}\exp\left(\frac{1}{2}\Omega^2\tau_1^{(2)}\right)\mu_1^{(2)} \\ \vdots \\ \mathrm{FT}\{\sqrt{S_{\mathrm{in}}(t)}\}\exp\left(\frac{1}{2}\Omega^2\tau_M^{(2)}\right)\mu_M^{(2)} \end{bmatrix}.
\end{aligned} \tag{19}
$$

Defining

$$
\left\langle P^{(1)}\right|\left|P^{(2)}\right\rangle = \begin{bmatrix} \kappa_{11} & \cdots & \kappa_{1M} \\ \vdots & \ddots & \vdots \\ \kappa_{M1} & \cdots & \kappa_{MM} \end{bmatrix}
$$

we can write (19) as

$$
\begin{aligned}
&Z^{(2)}(\Omega)\left\langle P^{(2)}\right||a\rangle \\
&= \sum_{j=1}^{M} \begin{bmatrix} \mathrm{FT}\{\sqrt{S_{\mathrm{in}}(t)}\}\kappa_{1j}\exp\left(\frac{1}{2}\Omega^2\tau_j^{(2)}\right)\mu_j^{(2)} \\ \vdots \\ \mathrm{FT}\{\sqrt{S_{\mathrm{in}}(t)}\}\kappa_{Mj}\exp\left(\frac{1}{2}\Omega^2\tau_j^{(2)}\right)\mu_j^{(2)} \end{bmatrix}
\end{aligned} \tag{20}
$$

[3]Fig. 1 would correspond more perfectly to (16) if drawn from right to left, but it is drawn here in the more familiar left-to-right form.

which shows that the output of the second-order system is the summation of M scaled and filtered copies of the input $S_{\mathrm{in}}(t)$. Referring to Fig. 1, we see that the output field $E_{\mathrm{out}}^{(2)}(t)$ is the result of (20) passing through the first-order system, which delays each term by the corresponding first-order GDs. As a result, at each first-order GD, we see a superposition of M pulses, which represent pulse broadening ∎

The pulse broadening caused by second-order modal dispersion is analogous to the polarization-dependent CD caused by second-order PMD [14].

Theorem 2-2: To second order, the input and output intensity waveforms, $S_{\mathrm{in}}(t)$ and $S_{\mathrm{out}}^{(2)}(t)$, are not related linearly.

Proof: Consider two input intensity waveforms, $S_{\mathrm{in}\text{-}1}(t)$ and $S_{\mathrm{in}\text{-}2}(t)$, and their sum, $S_{\mathrm{in}\text{-}3}(t) = S_{\mathrm{in}\text{-}1}(t)+S_{\mathrm{in}\text{-}2}(t)$. Assume that the normalized input pattern $|a\rangle$ does not change as the source is intensity-modulated. We would like to compute the corresponding output intensity waveforms to second order, $S_{\mathrm{out}\text{-}1}^{(2)}(t), S_{\mathrm{out}\text{-}2}^{(2)}(t)$ and $S_{\mathrm{out}\text{-}3}^{(2)}(t)$, and show that $S_{\mathrm{out}\text{-}3}^{(2)}(t) \neq S_{\mathrm{out}\text{-}1}^{(2)}(t) + S_{\mathrm{out}\text{-}2}^{(2)}(t)$. It is sufficient to prove nonlinearity for the system $D^{(2)}(t)^H D^{(2)}(t)$. Also, since time shifts of constituent pulses do not affect linearity, it is sufficient to show that $Z^{(2)}(t)^H Z^{(2)}(t)$ is nonlinear. By definition, the PMs are independent of frequency. Hence, converting (15) to the time domain, for inputs $k = 1, 2, 3$, we can write

$$
\begin{aligned}
Z_k^{(2)}(t) &= \left\langle P^{(1)}\right|\left|P^{(2)}\right\rangle \\
&\times \mathrm{FT}^{-1}\left\{Q^{(2)}(\Omega)\mathrm{FT}\{\sqrt{S_{\mathrm{in}\text{-}k}(t)}\}\right\}
\end{aligned} \tag{21}
$$

where the inverse Fourier transform is applied to each element of the diagonal operator $Q^{(2)}(\Omega)\mathrm{FT}\{\sqrt{S_{\mathrm{in}\text{-}k}(t)}\}$. Since $|P^{(k)}\rangle\langle P^{(k)}| = I$, and since the PMs are mutually orthogonal, we find

$$
\begin{aligned}
Z_k^{(2)}(t)^H Z_k^{(2)}(t) &= \mathrm{FT}^{-1}\left\{Q^{(2)}(\Omega)\mathrm{FT}\{\sqrt{S_{\mathrm{in}\text{-}k}(t)}\}\right\}^H \\
&\times \mathrm{FT}^{-1}\left\{Q^{(2)}(\Omega)\mathrm{FT}\{\sqrt{S_{\mathrm{in}\text{-}k}(t)}\}\right\}.
\end{aligned} \tag{22}
$$

As $Z_k^{(2)}(t)^H Z_k^{(2)}(t)$ is diagonal, it is described by the M elements

$$
\left(Z_k^{(2)}(t)^H Z_k^{(2)}(t)\right)_{jj} = |q_j(t) * \sqrt{S_{\mathrm{in}\text{-}k}(t)}|^2
$$
$$
\text{for } j = 1,\ldots,M \tag{23}
$$

where $q_j^{(2)}(\Omega) = \exp(1/2\Omega^2\tau_j^{(2)})$ are the elements of the second-order filter $Q^{(2)}(\Omega)$. In the absence of higher-order modal dispersion, these filters are impulses, $q_j(t) = C \cdot \delta(t)$
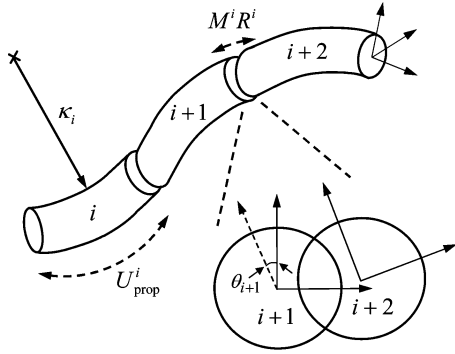
Fig. 2. Multimode fiber modeling. The fiber is divided into sections, each with random curvature and random orientation with respect to the previous section.

and the system is linear, as discussed earlier. But for a general filter $q_j(t)$, the inequality next holds[4]

$$\left| q_j^{(2)}(t) * \sqrt{S_{\text{in-1}}(t)} \right|^2 + \left| q_j^{(2)}(t) * \sqrt{S_{\text{in-2}}(t)} \right|^2$$
$$\neq \left| q_j^{(2)}(t) * \sqrt{S_{\text{in-1}}(t) + S_{in-2}(t)} \right|^2. \quad (24)$$

Hence, in general, $Z_k^{(2)}(t)^H Z_k^{(2)}(t)$ does not exhibit a linear input–output relationship. We conclude that the MMF does not exhibit a linear relationship between input and output intensity waveforms

$$\left| E_{\text{out-3}}^{(2)}(t) \right|^2 \neq \left| E_{\text{out-1}}^{(2)}(t) \right|^2 + \left| E_{\text{out-2}}^{(2)}(t) \right|^2$$
$$\text{or}$$
$$S_{\text{out-3}}^{(2)}(t) \neq S_{\text{out-1}}^{(2)}(t) + S_{\text{out-2}}^{(2)}(t).$$

∎

III. MODELING OF ALL-ORDER SYSTEM

Here, we confirm the analytical results of Section II and study modal dispersion beyond second order by performing numerical computations using our previously proposed model [20], which is modified here to incorporate higher-order effects.

A. MMF Modeling

Following [20], we model an MMF as a concatenation of many curved sections, as shown in Fig. 2. Each section lies in a plane, with the plane of one section rotated with respect to the previous section. The curvature in each section leads to both spatial-mode coupling and birefringence. The concatenation of many curved sections leads to polarization-dependent spatial-mode coupling. In our model, we do not assume any mechanism for mode-dependent loss.

Modal propagation is described by the propagation matrix for the entire fiber, $U_{\text{total}}(\omega)$. In deriving an expression for $U_{\text{total}}(\omega)$, we work with local normal modes [21]; thus, in each short section, we work in the basis of the ideal modes of an unperturbed fiber, with coordinate axes aligned along the plane of that particular section. Propagation in the ith section is affected by spatial-, but not by polarization-mode coupling, and is represented by a propagation matrix $U_i(\omega)$. At the junction between sections i and $i+1$, the local axes are rotated by an

angle θ_i. Two effects must be considered here. First, a polarization-rotation matrix R_i accounts for the polarization coupling due to axis rotation [20]. Second, the spatial-mode patterns that were defined along the previous axes must be expanded along the new axes to account for a new ideal mode basis. This is described by a spatial-mode projection matrix M_i [20]. It is easy to show that $[M_i, R_i] = 0$, which means that the order in which the two matrices are applied does not matter. Thus, for a total of N sections, we find the overall propagation matrix to be

$$U_{\text{total}}(\omega) = \prod_{i=1}^{N} M_i R_i U_i(\omega). \quad (25)$$

B. Numerical Results

Simulations have been done for a 50-μm-core graded-index silica MMF of total length $L = 1000$ m. The fiber has a numerical aperture (NA) = 0.19. At the wavelength $\lambda = 1550$ nm, there are 55 propagating modes in each polarization. The refractive index at the center of the fiber is $n_0 = 1.444$ at $\lambda = 1550$ nm. Away from this wavelength, n_0 is computed using the Sellmeier equation [22], [23]. The frequency derivative of the index, $dn_0/d\omega$, is also computed using the Sellmeier equation. Birefringence, defined as the difference between refractive indexes seen by x- and y-polarized waves, is assumed to be induced by stress due to curvature [25]

$$n_x - n_y = \delta \frac{C_s}{2k_0}(a\kappa)^2 \quad (26)$$

where δ is a birefringence scale factor, κ is the curvature of a fiber section, and C_s/k_0 is referred to as strain-optical coefficient. For an SMF, $C_s/k_0 = 0.0878\, n^3$ [23], and we should set $\delta = 1$. In MMF, birefringence and spatial-mode coupling do not necessarily have the same physical origins. In our model, both effects are induced by curvature; hence, in order to yield sufficient polarization-dependent spatial-mode coupling, the birefringence scale factor is set to $\delta = 8000$.[5] The fiber is divided into 10^3 sections, each 1 m long. Each section is rotated with respect to the previous one by an independent, identically distributed (i.i.d.) angle θ, whose probability density function (pdf) is normal with variance $\sigma_\theta^2 = 0.36$ rad^2. The curvature of each section is an i.i.d. random variable κ_i, whose pdf is the positive side of a normal pdf, and has variance σ_κ^2. As σ_κ^2 is increased, the model transitions from the low- to the medium- to the high-coupling regime.[6]

Similar to the experiments of [6], the input intensity waveform is a Gaussian pulse having a full-width at half-maximum of 10 ps, and the input electric field profile is a Gaussian mode of mode-field radius 8 μm, which is launched with a specified offset. In order to best reproduce the results in [6], the MMF refractive index exponent is chosen to be $\alpha = 1.84$.

Given an input intensity waveform, its square-root yields the input electric field waveform, which is Fourier-transformed to obtain the frequency components. In order to study all-order modal dispersion, the component at frequency ω

---

[4]Equation (24) is easily proven by counterexample, e.g., by letting $s_{\text{in-1}}(t)$ and $s_{\text{in-2}}(t)$ be adjacent but nonoverlapping rectangular pulses.

[5]For a typical curvature value $\kappa = 1$ m^{-1}, we obtain a birefringence $n_x - n_y \approx 7 \times 10^{-7}$, which is physically reasonable.

[6]Typical silica fibers correspond to the low-coupling regime [7], while typical plastic fibers correspond to the high-coupling regime [4]. We exclusively consider index profile parameters corresponding to silica fibers for the sake of consistency. Nonetheless, the case of high coupling is intended to qualitatively represent plastic fibers.
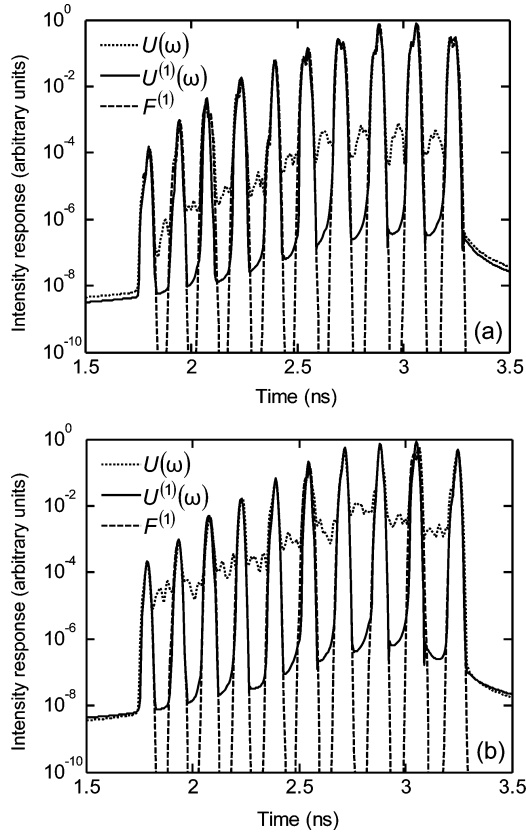
Fig. 3. Intensity pulse response in (a) low-coupling regime, $\sigma_\kappa^2 = 1.0$ m^{-2} and (b) medium-coupling regime, $\sigma_\kappa^2 = 1.7$ m^{-2}. The pulse response is computed using three different methods. $U(\omega)$: all-order propagation matrix, $U^{(1)}(\omega)$: first-order propagation matrix, and $F^{(1)}$: first-order PM model [20].

is propagated using the all-order propagation matrix $U(\omega)$. The propagated frequency components are summed up and inverse-Fourier-transformed to yield the output electric field waveform, whose squared magnitude yields the output intensity waveform. In order to study first-order modal dispersion, the first-order propagation matrix $U^{(1)}(\omega)$, calculated using (4) and (5), is used instead of $U(\omega)$. The output intensity waveform is also computed using the first-order PM model of [20], to facilitate comparison of our results to that model.

In order to study filling-in between peaks of the MMF intensity pulse response, we launched the input signal with an offset of 10.5 μm, similar to [6]. Fig. 3(a) shows intensity pulse responses computed for a curvature variance $\sigma_\kappa^2 = 1.0$ m^{-2}, corresponding to the low-coupling regime. The pulse response is computed using three different methods. $U(\omega)$ and $U^{(1)}(\omega)$ denote use of the all-order and first-order propagation matrices, respectively, while $F^{(1)}$ denotes use of the first-order PM model [20]. We observe that neither the first-order PM model $F^{(1)}$ nor the first-order propagation matrix $U^{(1)}(\omega)$ produces filling-in between the peaks,[7] while the all-order propagation matrix $U(\omega)$ produces an asymmetric filling-in similar to that observed in [6]. In Fig. 3(b), we have increased the curvature variance to $\sigma_\kappa^2 = 1.7$ m^{-2}, corresponding to the medium-coupling regime. As the mode coupling strength is

---

[7]In the case of the first-order propagation matrix $U^{(1)}(\omega)$, the apparent filling-in, which is orders of magnitude less than that of all-order system, is caused by numerical errors in the calculation of $F^{(1)}$ that appear in the phase of $U^{(1)}(\omega)$.
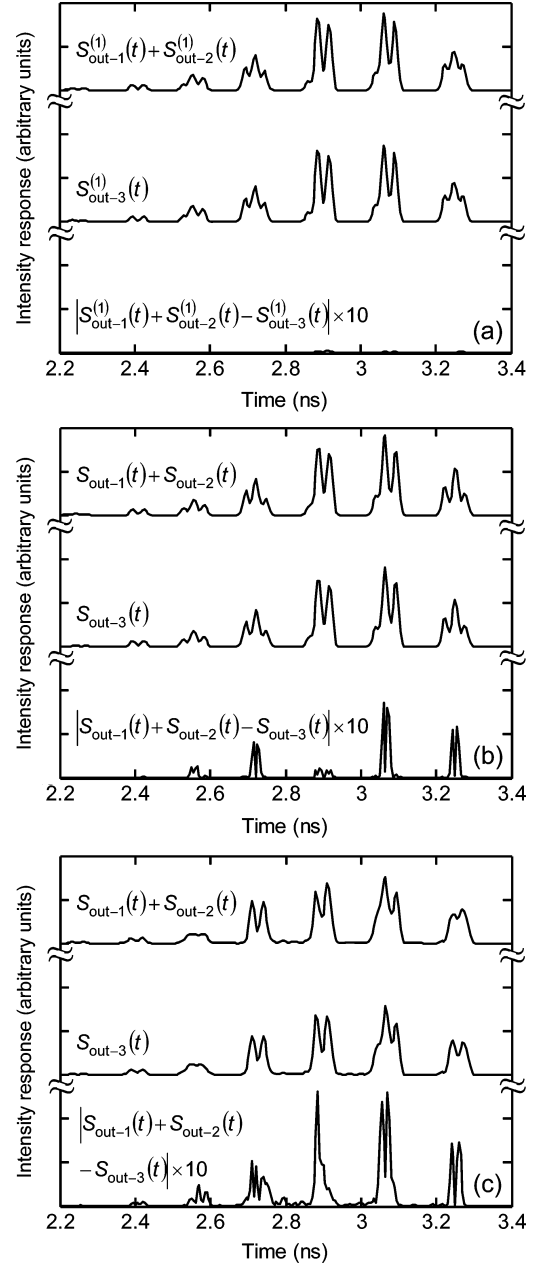

Fig. 4. Linearity test for: (a) first-order system, medium-coupling regime, $\sigma_\kappa^2 = 1.7$ m^{-2}, (b) all-order system, low-coupling regime, $\sigma_\kappa^2 = 1.0$ m^{-2}, and (c) all-order system, medium-coupling regime, $\sigma_\kappa^2 = 1.7$ m^{-2}.

increased, the filling-in produced by the all-order propagation matrix $U(\omega)$ becomes more pronounced.

In order to study the nonlinear intensity response of MMF, we have performed simulations analogous to the proof of Theorem 2-2. Input intensity waveforms $S_{\text{in-1}}(t)$ and $S_{\text{in-2}}(t)$ are 10-ps-wide Gaussian pulses that are offset by a 30 ps delay. The sum of these two input waveforms is $S_{\text{in-3}}(t) = S_{\text{in-1}}(t) + S_{\text{in-2}}(t)$. Signals are launched with an offset of 10.5 μm. The corresponding output intensity waveforms are $S_{\text{out-1}}(t), S_{\text{out-2}}(t)$, and $S_{\text{out-3}}(t)$, and $S_{\text{out-1}}(t) + S_{\text{out-2}}(t)$ is compared to $S_{\text{out-3}}(t)$. In Fig. 4(a), we consider the medium-coupling regime, $\sigma_\kappa^2 = 1.7$ m^{-2}, and compute the output waveforms using only the first-order propagation matrix $U^{(1)}(\omega)$ (hence the superscripts $^{(1)}$). We observe that $S_{\text{out-3}}^{(1)}(t) \approx S_{\text{out-1}}^{(1)}(t) + S_{\text{out-2}}^{(1)}(t)$, confirming
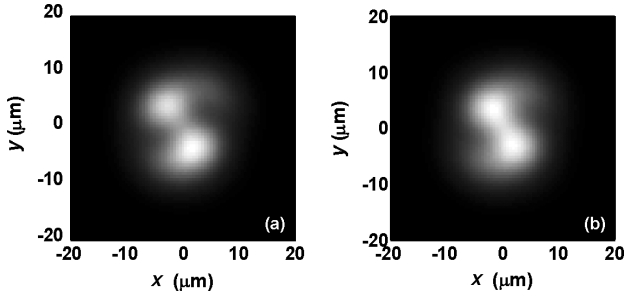
Fig. 5. Time-average output intensity pattern for a 10-ps Gaussian pulse launched with 6.4-μm offset into a 1-km fiber with $\sigma_\kappa^2 = 1.9$ m^{-2}: (a) first-order system and (b) all-order system.
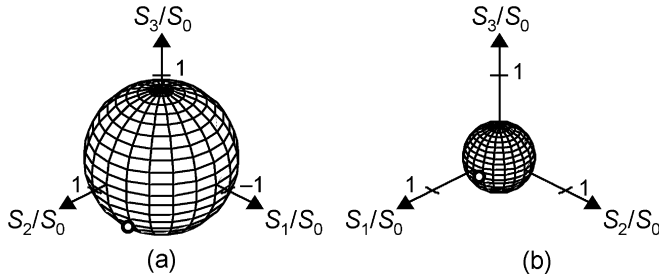

Fig. 6. Time-average output polarization for a 10-ps Gaussian pulse launched with 2.4 μm offset into a 1-km fiber with $\sigma_\kappa^2 = 0.48$ m^{-2}: (a) first-order system and (b) all-order system.

linearity of the first-order response, as predicted in Section II-A. In Fig. 4(b) and (c), we consider the low- and medium-coupling regimes, $\sigma_\kappa^2 = 1.0$ m^{-2} and $\sigma_\kappa^2 = 1.7$ m^{-2}, and compute the outputs using the all-order propagation matrix $U(\omega)$. In both cases, we see that $S_{\text{out-3}}(t) \neq S_{\text{out-1}}(t) + S_{\text{out-2}}(t)$, demonstrating the nonlinear intensity response of MMF caused by higher-order modal dispersion. Comparing Fig. 4(b) and (c), we see that the nonlinearity becomes more pronounced as the mode-coupling strength is increased, since the nonlinearity arises from "mode-dependent CD," which is analogous to polarization-dependent CD in SMF with higher-order PMD [17]. We emphasize that the nonlinear intensity response is not a consequence of the particular multisection model used for our numerical calculations; it is a general property of systems in which the field-propagation operator phase response exhibits higher-order frequency dependence.

It is known that in SMF, higher-order PMD leads to depolarization [24]. Our simulations show that in MMF, higher-order modal dispersion causes analogous effects, which are blurring of the output intensity pattern and depolarization of the output. Fig. 5. shows time-average output intensity patterns for a 10-ps Gaussian pulse that has been launched with 6.4-μm offset, in the medium-coupling regime, $\sigma_\kappa^2 = 1.9$ m^{-2}. Fig. 5(a) uses the first-order propagation matrix $U^{(1)}(\omega)$, while Fig. 5(b) uses the all-order $U(\omega)$. Comparing these two, we see that higher-order modal dispersion causes output pattern blurring. Fig. 6 shows the time-average output Stokes parameters for a 10-ps Gaussian pulse that has been launched with 2.4-μm offset, in the low-coupling regime, $\sigma_\kappa^2 = 0.48$ m^{-2}. Fig. 6(a) uses the first-order propagation matrix $U^{(1)}(\omega)$, and the output is nearly fully polarized.[8] Fig. 6(b) uses the all-order $\mathbf{U}(\omega)$, and the output is depolarized significantly.

[8] It was demonstrated in [20] that even first-order modal dispersion in the low-coupling regime can cause some depolarization.

IV. CONCLUSION

We have studied higher-order modal dispersion in MMF. Through analysis, we showed that to first order in frequency, the input and output intensity waveforms are related linearly, and the intensity pulse response consists of discrete peaks. We also showed that to second order, the input–output intensity response is nonlinear, and the intensity pulse response exhibits pulse broadening, effects analogous to SMF with higher-order PMD. We have performed numerical simulations modeling an MMF as a concatenation of short sections, each having random curvature and random angular orientation. The model includes both spatial- and polarization-mode couplings, and allows us to study all-order modal dispersion. Through simulation, we confirmed the results of our first- and second-order analyses. We demonstrated that higher-order modal dispersion leads to a nonlinear input–output intensity response, and causes filling-in between peaks in the intensity pulse response. Higher order modal dispersion also causes pattern blurring and depolarization of the output, which are analogous to depolarization in SMF with higher-order PMD. While experiments have confirmed the filling-in of the intensity pulse response [6], further experiments may help quantify the nonlinearity of the input–output intensity response. Inclusion of this nonlinear response may lead to refined modeling of high-speed links in MMF.

REFERENCES

[1] K.-I. Kitayama, S. Sikai, and N. Uchida, "Impulse response prediction based on experimental mode-coupling coefficient in a 10-km long graded-index fiber," *J. Quantum Electron.*, vol. QE-16, no. 3, pp. 356–362, Mar. 1980.

[2] R. Olshansky, "Mode-coupling effects in graded-index optical fibers," *Appl. Opt.*, vol. 14, no. 4, pp. 935–945, Apr. 1975.

[3] D. Gloge, "Optical power flow in multimode fibers," *Bell Syst. Tech. J.*, vol. 51, no. 8, pp. 1767–1780, Oct. 1972.

[4] A. F. Garito, J. Wang, and R. Gao, "Effects of random perturbations in plastic optical fibers," *Science*, vol. 281, pp. 962–967, Aug. 1998.

[5] R. Olshansky and D. B. Keck, "Pulse broadening in graded-index optical fibers," *Appl. Opt.*, vol. 15, no. 2, pp. 483–491, Feb. 1976.

[6] K. Balemarthy, A. Polley, and S. E. Ralph, "Electronic equalization of multi kilometer 10-Gb/s multimode fiber links: Mode-coupling effects," *J. Lightw. Technol.*, vol. 24, no. 12, pp. 4885–4893, Dec. 2006.

[7] X. Shen, J. M. Kahn, and M. A. Horowitz, "Compensation for multimode fiber dispersion by adaptive optics," *Opt. Lett.*, vol. 30, no. 22, pp. 2985–2987, Nov. 2005.

[8] C. D. Poole, "Statistical treatment of polarization dispersion in single-mode fiber," *Opt. Lett.*, vol. 13, no. 8, pp. 687–689, Aug. 1988.

[9] C. D. Poole and R. E. Wagner, "Phenomenological approach to polarization dispersion in long single-mode fibers," *Electron. Lett.*, vol. 22, no. 19, pp. 1029–1030, Sep. 1986.

[10] D. A. Nolan and M. J. Li, "Fiber spin-profile designs for producing fibers with low polarization mode dispersion," *Opt. Lett.*, vol. 23, no. 21, pp. 1659–1661, Nov. 1998.

[11] D. A. Nolan, X. Chen, and M. J. Li, "Fibers with low polarization-mode dispersion," *J. Lightw. Technol.*, vol. 22, no. 4, pp. 1066–1076, Apr. 2004.

[12] A. Djupsjöbacka, "On differential group-delay statistics for polarization-mode dispersion emulators," *J. Lightw. Technol.*, vol. 19, no. 2, pp. 285–290, Feb. 2001.

[13] R. Khosravani, I. T. Lima, P. Ebrahimi, E. Ibragimov, A. E. Willner, and C. R. Menyuk, "Time and frequency domain characteristics of polarization-mode dispersion emulators," *IEEE Photon. Technol. Lett.*, vol. 13, no. 2, pp. 127–129, Feb. 2001.

[14] A. Eyal, W. K. Marshal, M. Tur, and A. Yariv, "Representation of second-order polarization mode dispersion," *Electron. Lett.*, vol. 35, no. 19, pp. 1658–1659, Sep. 1999.

[15] H. Kogelnik, L. E. Nelson, J. P. Gordon, and R. M. Jopson, "Jones matrix for second-order polarization mode dispersion," *Opt. Lett.*, vol. 25, no. 1, pp. 19–21, Jan. 2000.

[16] A. Orlandini and L. vincetti, "A simple and useful model for Jones matrix to evaluate higher-order polarization-mode dispersion effects," *IEEE Photon. Technol. Lett.*, vol. 13, no. 11, pp. 1176–1178, Nov. 2001.

[17] E. Forestieri and L. vincetti, "Exact evaluation of the Jones matrix of a fiber in the presence of polarization mode dispersion of any order," *J. Lightw. Technol.*, vol. 19, no. 12, pp. 1898–1909, Dec. 2001.

[18] M. F. Ferreira, "Evaluation of higher-order PMD effects using Jones matrix analytical models: A comparative study," *Proc. SPIE*, vol. 6193, pp. 619308-1–619308-9, May 2006.

[19] S. Fan and J. M. Kahn, "Principal modes in multimode waveguides," *Opt. Lett.*, vol. 30, no. 2, pp. 135–137, Jan. 2005.

[20] M. B. Shemirani, W. Mao, R. A. Panicker, and J. M. Kahn, "Principal modes in graded-index multimode fiber in presence of spatial- and polarization-mode-coupling," *J. Lightw. Technol.*, vol. 27, no. 10, pp. 1248–1261, May 2009.

[21] D. Marcuse, *Theory of Dielectric Optical Waveguides*. New York: Academic, 1974, ch. 3.

[22] G. Ghosh and H. Yajima, "Pressure-dependent Sellmeier coefficients and material dispersions for silica fiber glass," *J. Lightw. Technol.*, vol. 16, no. 11, pp. 2002–2005, Nov. 1998.

[23] K. Iizuka, *Elements of Photonics in Free Space and Special Media*. New York: Wiley, 2002, p. 383.

[24] G. J. Foschini, L. E. Nelson, R. M. Jopson, and H. Kogelnik, "Probability densities of second-order polarization mode dispersion including polarization dependent chromatic fiber dispersion," *IEEE Photon. Technol. Lett.*, vol. 12, no. 3, pp. 293–295, Mar. 2000.

[25] S. C. Rashleigh, "Origins and control of polarization effects in single-mode fibers," *J. Lightw. Technol.*, vol. LT-1, no. 2, pp. 312–331, Jun. 1983.

Mahdieh B. Shemirani received the B.Sc. degree in electrical engineering from Sharif University of Technology, Tehran, Iran, in 2004, and the M.Sc. degree in electrical engineering in 2006 from Stanford University, Stanford, CA, where she is currently working toward the Ph.D. degree in electrical engineering.

Her current interests include fiber modeling, performance optimization of optical communication systems using adaptive optics, and designing analog Fourier transform processors in RF domain.

Dr. Shemirani is the recipient of Stanford Graduate Fellowship in 2004.

Joseph M. Kahn (M'90–SM'98–F'00) received the A.B., M.A., and Ph.D. degrees in physics from the University of California, Berkeley, in 1981, 1983, and 1986, respectively.

From 1987 to 1990, he was at AT&T Bell Laboratories, Crawford Hill Laboratory, Holmdel, NJ. He was engaged in demonstration of multi-Gb/s coherent optical fiber transmission systems, setting world records for receiver sensitivity. From 1990 to 2003, he was a member of the faculty in the Department of Electrical Engineering and Computer Sciences, University of California, Berkeley, where he was involved in research on optical and wireless communications. Since 2003, he has been a Professor of electrical engineering at Stanford University, Stanford. His current research interests include single- and multimode optical fiber communications, free-space optical communications, and microelectromechanical systems for optical communications.

Prof. Kahn received the National Science Foundation Presidential Young Investigator Award in 1991. From 1993 to 2000, he was a Technical Editor of the IEEE PERSONAL COMMUNICATIONS MAGAZINE. Since 2009, he has been an Associate Editor of the IEEE/OSA JOURNAL OF OPTICAL COMMUNICATIONS AND NETWORKING. In 2000, he helped found StrataLight Communications (now Opnext Subsystems), where he was the Chief Scientist from 2000 to 2003.